Replacement of the Proximal Histidine Iron Ligand by a Cysteine or Tyrosine Converts Heme Oxygenase to an Oxidase†

Yi Liu,‡ Pierre Moënne-Loccoz,§ Dean P. Hildebrand,|| Angela Wilks,‡ Thomas M. Loehr,§ A. Grant Mauk,|| and Paul R. Ortiz de Montellano*,‡

Department of Pharmaceutical Chemistry, School of Pharmacy, University of California, San Francisco, California 94143-0446, Department of Biochemistry and Molecular Biology, Oregon Graduate Institute of Science and Technology, P.O. Box 91000, Portland, Oregon 97291-1000, and Department of Biochemistry & Molecular Biology, The University of British Columbia, 2146 Health Sciences Mall, Vancouver, British Columbia Canada V6T 1Z3

Received November 12, 1998; Revised Manuscript Received January 13, 1999

ABSTRACT: The H25C and H25Y mutants of human heme oxygenase-1 (hHO-1), in which the proximal iron ligand is replaced by a cysteine or tyrosine, have been expressed and characterized. Resonance Raman studies indicate that the ferric heme complexes of these proteins, like the complex of the H25A mutant but unlike that of the wild type, are 5-coordinate high-spin. Labeling of the iron with ^{54}Fe confirms that the proximal ligand in the ferric H25C protein is a cysteine thiolate. Resonance-enhanced tyrosinate modes in the resonance Raman spectrum of the H25Y·heme complex provide direct evidence for tyrosinate ligation in this protein. The H25C and H25Y heme complexes are reduced to the ferrous state by cytochrome P450 reductase but do not catalyze α-*meso*-hydroxylation of the heme or its conversion to biliverdin. Exposure of the ferrous heme complexes to O_2 does not give detectable ferrous−dioxy complexes and leads to the uncoupled reduction of O_2 to H_2O_2. Resonance Raman studies show that the ferrous H25C and H25Y heme complexes are present in both 5-coordinate high-spin and 4-coordinate intermediate-spin configurations. This finding indicates that the proximal cysteine and tyrosine ligand in the ferric H25C and H25Y complexes, respectively, dissociates upon reduction to the ferrous state. This is confirmed by the spectroscopic properties of the ferrous−CO complexes. Reduction potential measurements establish that reduction of the mutants by NADPH−cytochrome P450 reductase, as observed, is thermodynamically allowed. The two proximal ligand mutations thus destabilize the ferrous−dioxy complex and uncouple the reduction of O_2 from oxidation of the heme group. The proximal histidine ligand, for geometric or electronic reasons, is specifically required for normal heme oxygenase catalysis.

Heme oxygenase catalyzes the NADPH- and cytochrome P450 reductase-dependent oxidation of heme[1] to biliverdin and CO (*1*) (Scheme 1). The enzyme, which employs heme as both the prosthetic group and substrate, regiospecifically oxidizes the heme at the α-*meso* position. This enzyme is physiologically important, in addition to its role in iron homeostasis (*2*), because of the biological properties of its two organic reaction products. Biliverdin, after reduction to bilirubin by biliverdin reductase, is normally excreted as a glucuronic acid conjugate (*3*). Whereas low bilirubin levels may serve as a physiological antioxidant (*4*), impairment of the excretion of bilirubin due to glucuronyl transferase deficiencies, as is found in many neonates and in individuals with gene defects, can lead to the accumulation of neurotoxic levels of bilirubin (*5*). Approaches to the prevention of bilirubin accumulation, including the inhibition of heme

Scheme 1: Reaction Intermediates in the Heme Oxygenase-Catalyzed Oxidation of Heme to Biliverdin[a]

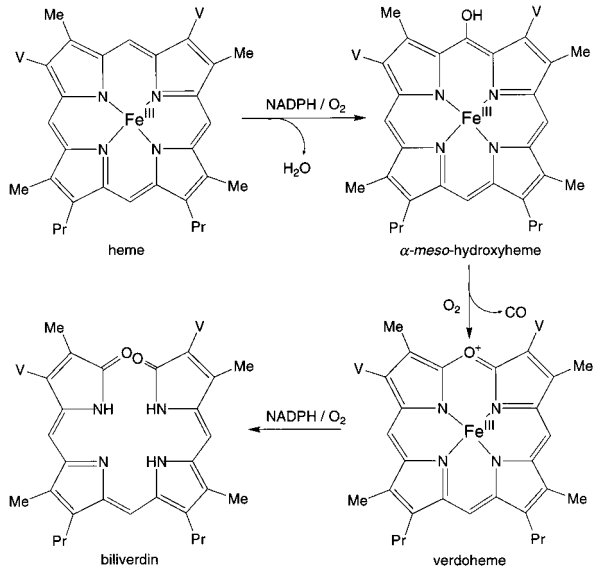

[a] The substituents on the porphyrin are vinyl (V) and propionate (Pr).

† This work was supported by National Institutes of Health Grants DK30297 (P.R.O.M.) and GM34468 (T.M.L.) and by Medical Research Council of Canada Grant MT-7182 (A.G.M.).

* To whom correspondence should be addressed: FAX (415) 502-4728; Email ortiz@cgl.ucsf.edu.

‡ University of California, San Francisco.

§ Oregon Graduate Institute of Science and Technology.

|| University of British Columbia.

[1] Abbreviations: HO-1, heme oxygenase isoform 1; hHO-1, truncated human HO-1; heme, iron protoporphyrin IX regardless of oxidation and ligation state; RR, resonance Raman; 5c and 6c, five-coordinate and six-coordinate, respectively; HS, LS, and IS, high-spin, low-spin, and intermediate-spin, respectively.

10.1021/bi982707s CCC: $18.00
Published on Web 03/04/1999

oxygenase, are therefore of clinical interest (*6*−*8*). More recently, the CO produced by heme oxygenase has emerged as a potentially important signaling molecule akin to nitric oxide (*9*−*12*).

The existence of two heme oxygenase isoforms, denoted HO-1 and HO-2, is now well established (*5, 13, 14*), and a third isoform whose significance is unclear has been reported (*15*). HO-1 is inducible by a variety of chemical agents and a range of stress conditions; it is found in highest concentrations in the spleen and liver. HO-2 is not induced by such exogenous stimuli and is found in highest concentration in the brain and testes. The heme oxygenases are membrane-bound proteins (*16, 17*), but water-soluble, catalytically active versions of rat and human HO-1 without the 23 C-terminal amino acid membrane anchor have been expressed in *Escherichia coli* (*18, 19*).

His-25 has been identified as the proximal iron ligand in the heme·hHO-1 complex by site-directed mutagenesis and RR spectroscopy (*20*−*25*). Replacement of the proximal histidine residue by an alanine produces a catalytically inactive protein that binds heme without providing a strong axial iron ligand (*21*). The role of His-25 as the proximal iron ligand was confirmed by recovery of the enzymatic activity when an imidazole was bound to the heme·H25A mutant (*22*).

The proximal iron ligand plays an important role in controlling the chemistry and the function of the various classes of hemoproteins. Three amino acids are found as hemoprotein proximal ligands: histidine (e.g., peroxidases), tyrosine (catalases), and cysteine (e.g., cytochromes P450). The ligands differ in their electron-donating properties, with thiolate as the most and tyrosinate as the least electron-donating group. For histidine ligands, the electron-donating properties of the imidazole group can be enhanced by increasing its imidazolate character through hydrogen bonding. In the case of the cytochromes P450, the activated oxygenating intermediate is thought to be a high-valent iron−oxo species generated by heterolysis of the O−O bond of the hydroperoxoiron(III) complex. Strong donation from the proximal cysteine thiolate ligand and protonation of the oxygen by a distal hydrogen-bonding network destabilizes the dioxygen bond toward heterolytic cleavage (*26*). A related push/pull mechanism operates in the peroxidases, in which a strongly hydrogen-bonded proximal histidine and a distal histidine and positively charged arginine facilitate heterolytic cleavage of the dioxygen bond. However, in heme oxygenase, the reaction that yields α-*meso*-hydroxyheme is thought to involve electrophilic addition of the distal oxygen of the iron-bound peroxide to the porphyrin ring (*18, 27*). The fact that reaction of heme oxygenase with bulky alkyl and acylhydroperoxides produces a compound II-like ferryl species and a protein radical but no verdoheme or biliverdin precludes the ferryl species from a role in heme α-*meso*-hydroxylation (*18*). The absence of strong hydrogen bonding by the proximal histidine in heme oxygenase (*20*) may impair ferryl formation and allow a competitive reaction with the heme to occur.

To examine the role of the proximal ligand in the heme oxygenase mechanism, particularly on electron transfer and α-*meso*-hydroxylation, we have replaced the proximal histidine ligand of human heme oxygenase 1 (hHO-1) with a cysteine (H25C) and a tyrosine (H25Y), the ligands present in P450 and catalase, respectively. In this paper, we report the preparation, characterization, reaction with peroxides, reduction potentials, electron-transfer properties, and catalytic properties of the H25C and H25Y mutants. We find that replacement of the proximal histidine ligand by a cysteine or tyrosine allows the first electron transfer to the heme but suppresses α-*meso*-hydroxylation. After the first electron transfer, the two mutants, like the proximal H25A mutant, give rise to H_2O_2 through an uncoupled reaction pathway that does not yield α-*meso*-hydroxyheme. Spectroscopic data suggests that dissociation of the proximal ligand of the two mutants upon reduction of the iron destabilizes the ferrous dioxygen heme complex.

EXPERIMENTAL PROCEDURES

Materials. H_2O_2 (30%), NADPH, heme, protoporphyrin IX, bovine serum albumin, sodium dithionite, protocatechuate, 2-hydroxy-1,4-naphthoquinone, and pyridine were obtained from Aldrich or Sigma. High-purity argon (99.998%) and CO (99.95%) were obtained from Matheson, and high-purity O_2 (99.6%) was from Aldrich. All chemicals were used without further purification.

General Methods. The hHO-1 construct that was used encoded the human protein without the 23 N-terminal amino acids (*19*). Oligonucleotide synthesis was carried out by the Biomolecular Resource Center of the University of California at San Francisco on an Applied Biosystems 380B DNA synthesizer. Plasmid purification, sequencing, subcloning, and bacterial transformations were carried out by standard procedures (*28*). *Escherichia coli* strain DH5α [F′ *ara* Δ*(lac*−*proAB)rpsL* φ80d *lacZ*ΔM15 *hsdR17*] was used for expression of the hHO-1 constructs. Deionized, doubly distilled water was used for all experiments. HPLC was done on a Hewlett-Packard Series II 1090 liquid chromatograph. UV−vis spectra were recorded on a Cary Varian Model 1E spectrophotometer.

Mutagenesis. The hHO-1 H25C mutant was generated with the Altered Site II mutagenesis kit (Promega, Madison, WI). The H25Y hHO-1 mutant was generated with the QuickChange site-directed mutagenesis kit (Stratagene). Antibiotic selection (ampicillin) was used to obtain a high frequency of mutants. Transformants were screened by restriction digestion and confirmed by sequence analysis.

Expression, Purification, Protein Assay, and Characterization of the Proximal hHO-1 Mutants. The H25C and H25Y heme·hHO-1 complexes were expressed in *Escherichia coli* and were purified as previously reported for the wild-type protein (*18*). The catalytic activity of heme oxygenase was assayed at 37 °C in the presence of rat liver biliverdin reductase by monitoring the absorbance increase at 468 nm due to bilirubin. The biliverdin products were analyzed by HPLC as previously described (*18*), and their optical spectra were obtained in 100 mM potassium phosphate buffer (pH 7.4). The ferrous and ferrous−CO complexes were formed by reduction of the ferric complexes with sodium dithionite or, anaerobically, with NADPH−cytochrome P450 reductase followed by the addition of CO.

Aerobic and Anaerobic Reaction of the Heme-Proximal Mutant Complexes with H_2O_2. Anaerobic techniques were as previously reported (*29*). The reconstituted heme−H25C or H25Y hHO-1 complex (35 μM in 1.2 mL of 100 mM

potassium phosphate buffer, pH 7.4) was placed in a custom-made anaerobic UV cuvette and 1 equiv of H_2O_2 (50 μL) was placed in the sidearm of the cuvette. The concentration of H_2O_2 was quantitated by titration with iodide (*30*) or by spectrophotometry (ϵ_{240} = 43.6 M^{-1} cm^{-1}). The protein solution and H_2O_2 were made anaerobic by flushing the cuvette with oxygen-free argon for at least 40 min. The reaction was initiated by anaerobically mixing the protein solution with the H_2O_2 in the sidearm at 23 °C, and the UV−vis spectrum was recorded until no further changes occurred. For aerobic experiments, parallel reaction conditions were used in the presence of air.

Synthesis of [^{54}Fe]Heme. The heme synthesis method is similar to that previously described (*31*). ^{54}Fe foil (10 mg), purchased from Pennwood Chemicals, was cut into small pieces and dissolved anaerobically in concentrated HCl. After the metal completely dissolved, the solution was evacuated under a stream of Ar. Anhydrous ^{54}Fe ferrous chloride was thus obtained and stored in a desiccator. Protoporphyrin IX (25 mg) in 50 mL of *N*,*N*-dimethylformamide (DMF) was continually bubbled with Ar and heated to reflux for 10 min. ^{54}Fe ferrous chloride, anaerobically dissolved in H_2O, was added to the refluxing protoporphyrin IX solution. The reaction was allowed to reflux for a further 15 min before the heme solution was cooled to room temperature and exposed to air with constant stirring for 20 min. The heme product was extracted by adding a 5-fold volume of ether. Excess ferric salts and DMF were removed by liquid-phase extractions with an equal volume of 0.1 N HCl containing 0.1 N NaCl. Unreacted porphyrin was extracted with an equal volume of 1 N HCl. The ether phase was washed to neutrality with H_2O and then evaporated to dryness. The heme residue was stored at −20 °C. The absorption spectrum of the heme product was measured by addition of 20% pyridine to the ferrous heme in 0.2 N NaOH.

Resonance Raman Spectroscopy. Typical enzyme concentrations for RR experiments were 150−250 μM in 100 mM potassium phosphate (pH 7.4) buffer solution. Reduction to the ferrous state was achieved by adding microliter aliquots of a 10 mM sodium dithionite solution to an argon-purged sample in the Raman capillary cell and was monitored by UV−vis spectroscopy in the same cell (*32*). ^{12}CO (CP grade, Air Products) and ^{13}CO (99% ^{13}C, Cambridge Isotope Laboratory) adducts were obtained by injecting CO through a septum into a closed capillary containing argon-purged, reduced enzyme (∼20 μL).

RR spectra were obtained on a custom McPherson 2061/207 spectrograph (set at 0.67 m with variable gratings) equipped with a Princeton Instruments liquid-N_2-cooled (LN-1100PB) CCD detector. Kaiser Optical supernotch filters were used to attenuate Rayleigh scattering. Excitation sources consisted of an Innova 302 krypton laser (413 nm) and a Coherent Innova 90-6 argon laser (514.5 nm). Spectra were collected in a 90°-scattering geometry on samples at room temperature with a collection time of a few minutes. Frequencies were calibrated relative to indene and CCl_4 standards and are accurate to ±1 cm^{-1}. CCl_4 was also used to check the polarization conditions. Optical absorption spectra of the Raman samples were obtained on a Perkin-Elmer Lambda 9 spectrophotometer to monitor the samples (fully oxidized, fully reduced, CO complex) both before and after laser illumination.

Uncoupled Oxidation of the Heme·hHO-1 Proximal Mutant Complexes. The rate of uncoupled oxidation of the proximal mutants was determined by measuring the rate of formation of H_2O_2. Under the same conditions, the rates of oxygen and NADPH consumption by the mutant were also determined. The chemical and protein concentrations used in the kinetic assays were the following: 1 or 5 μM protein in 100 mM potassium phosphate buffer, pH 7.4, with variable (substoichiometric and stoichiometric) amounts of cytochrome P450 reductase in the presence of 100 μM heme/3 μM bovine serum albumin. For determination of the NADPH consumption rate, the protein solution was placed in a 0.2-cm path length fluorescence cuvette thermostated to 25 °C. The reaction was initiated by addition of 0.5 mM NADPH, and the rate was measured by monitoring the absorption decrease at 340 nm (ϵ = 6.22 mM^{-1} cm^{-1}). Parallel experiments were carried out for measurement of the oxygen consumption rate at 25 °C using a Gilson Oxy5 Oxygraph electrode. The oxygen electrode was calibrated by turning over 1 nmol of protocatechuate with protocatechuate 3,4-dioxygenase at 25 °C. The H_2O_2 formation rate was determined by subtracting the oxygen consumption rate of the H25C mutant in the absence of catalase from that in the presence of catalase and then multiplying the value by a factor of 2 (catalase reacts with 1 mol of H_2O_2 to generate $^1/_2$ mol of O_2). Since 1 mol of NADPH will generate 1 mol of H_2O_2 if the reaction is fully uncoupled, the percentage of uncoupled reaction is given by the ratio of the rates of H_2O_2 formation and NADPH consumption. Initial reaction rates were used for all of these measurements.

Spectroelectrochemical Reduction Potential Measurements. Electrochemical measurements were performed with an electrochemical cell constructed from glass to which an optically transparent thin-layer electrode (OTTLE) constructed from quartz was attached with a graded seal. The design of this cell was essentially the design of the cell described by Stankovich (*33*) except that the optical path length of our cell was ∼0.2 mm. The maintenance of strictly anaerobic conditions throughout the titration is necessary to avoid the catalytic conversion of heme to biliverdin. The reconstituted heme·hHO-1 complex in 20 mM potassium phosphate buffer, pH 7.4 (90−100 μM, 7 mL) was placed in a serum bottle fitted with a serum cap. The protein sample was purged with O_2-free Ar for 1 h. The mediators (see below) were then added quickly to the sample and purging was continued for another hour. The sample was kept on ice to prevent denaturation of the protein. The sample was loaded into the OTTLE cell in a glovebox and sealed with a serum cap fitted with microbore tubing for purging with nitrogen, a platinum working electrode, and a stoppered glass frit for introduction of the standard calomel reference electrode (SCE) (Radiometer Model 4112).

The OTTLE assembly was placed into a water-jacketed cell holder mounted in the sample compartment of a Cary Model 219 spectrophotometer, and a slow stream of O_2-free argon was passed over the solution throughout the titration. A circulating water bath was used to maintain constant temperature (25 °C). Sample temperature was monitored with a subminiature copper−constantan thermocouple and a digital thermometer (Fluke Model 2175A). Solution potential was controlled with a Princeton Applied Research Model 173 potentiostat and measured with a Keithley Model 177

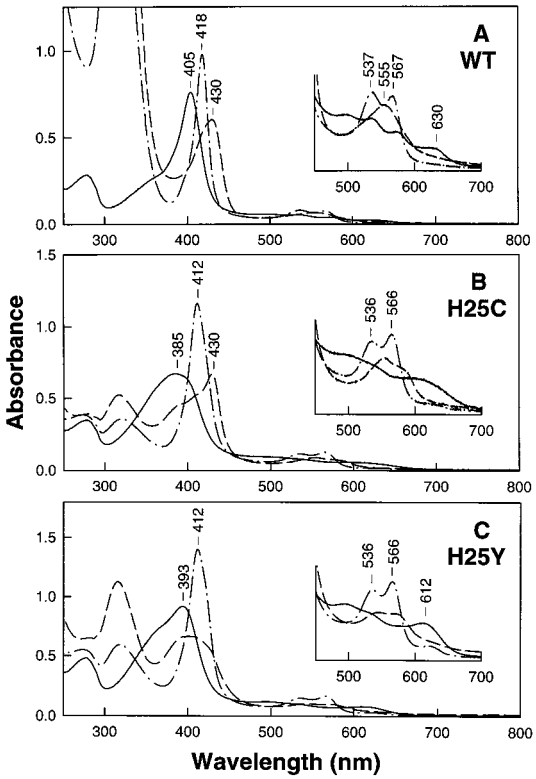

FIGURE 1: UV−vis spectra of the wild-type (A), H25C (B), and H25Y (C) heme·hHO-1 complexes in the ferric (—), ferrous (– – –), and ferrous−CO (– · –) states. The insert in each panel is a 5-fold expansion in the absorbance of the region between 500 and 700 nm. The ferrous protein was generated by the addition of excess sodium dithionite to the ferric protein. The ferrous−CO complex was generated by exposure of the reduced protein to CO.

digital microvoltmeter. Potentials were referred to the standard hydrogen electrode (SHE) according to Dutton (*34*). The SCE was standardized against a saturated solution of quinhydrone in 20 mM potassium phosphate (pH 7.4, 25 °C).

Three mediators were used in varying combinations to permit facile coupling of the heme oxygenase and its variants to the gold working electrode. For wild-type heme oxygenase, H25A−monoimidazole, and H25A−bis(imidazole) heme oxygenase complexes, a solution containing 20% molar equivalents of $[Ru(NH_3)_6]Cl_3$ (Strem Chemicals), $[Ru(NH_3)_5Im]Cl_3$ (*35*), and 2-hydroxy-1,4-naphthaquinone was added to the protein. For the H25A variant, 20% molar equivalents of 2-hydroxy-1,4-naphthaquinone, anthraquinone-2-sulfonate (ICN Pharmaceuticals), and benzyl viologen were used.

RESULTS

Expression and Purification of the H25C and H25Y Heme·hHO-1 Mutant Complexes. The purification procedure was the same as previously described for wild-type hHO-1 (*18*). The preparation of the H25C heme·hHO-1 complex yields two fractions in the final heme reconstitution step of the purification sequence. The two fractions were separated on a hydroxyapatite column eluted with a potassium phosphate gradient (10−140 mM, pH 7.4). The first fraction (70%) of the ferric H25C heme·hHO-1 complex had a Soret maximum at 385 nm (Figure 1B) and the later fraction (30%) had a corresponding maximum at 400 nm (not shown). In contrast, a single fraction with a Soret maximum at 393 nm (Figure 1C) was obtained for the H25Y heme·hHO-1 complex.

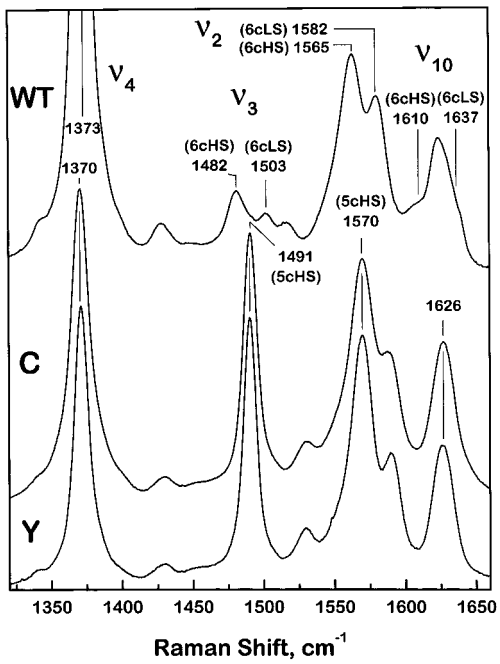

FIGURE 2: High-frequency region of the RR spectra of the ferric wild-type (WT), H25C (C), and H25Y (Y) heme·hHO-1 complexes. Spectra were obtained at room temperature with 413-nm excitation (5 mW).

Further spectroscopic characterization of the H25C samples established that only the major fraction (λ_{max} = 385 nm) has the desired Fe−S ligation.[2] The protein yields for both the H25C and H25Y mutants were lower (∼2−3 mg/L) than those previously obtained with wild-type hHO-1 (*19*). Unlike the ferrous heme in the wild-type protein, both proximal mutants have broad Soret absorption bands indicative of a mixture of coordination states. However, the ferrous−CO spectra of the H25C and H25Y heme complexes have nearly identical optical spectra with Soret maxima at 412 nm for the ferrous−CO complexes (Figure 1B,C). The latter are also similar to the Soret band of the heme−CO complex of the H25A mutant (*21*). Neither of the two proximal ligand mutants was catalytically active in terms of biliverdin formation: the H25C and H25Y hHO-1 complexes exhibit no more than ∼0.8% and 1.5%, respectively, of the wild-type heme·hHO-1 activity when bilirubin formation is monitored at 37 °C.

Resonance Raman Characterization of the Coordination and Spin States of the Ferric H25C and H25Y Heme·hHO-1 Complexes. The high-frequency regions of the RR spectra of the wild-type, H25C, and H25Y heme·hHO-1 complexes obtained with Soret excitation are dominated by the totally symmetric modes of the porphyrin ring (Figure 2). The RR frequencies (*36*) observed in the wild-type enzyme are characteristic of a 6-coordinate high-spin/low-spin mixture (ν_2 at 1565 and 1582, ν_3 at 1482 and 1503, ν_4 at 1373, ν_{10} at 1610 and 1637 cm^{-1}), consistent with binding to the iron of a water molecule (or an OH^- depending on the buffer pH) in addition to the proximal histidine (*20*, *23*, *24*). Both mutated proteins show RR spectra indicative of a pure

[2] Resonance Raman spectra of the two fractions of the heme·H25C mutant show that both fractions are 5-coordinate high-spin heme, but only the 385-nm fraction has the RR band at 348 cm^{-1} indicative of Fe−S ligation.

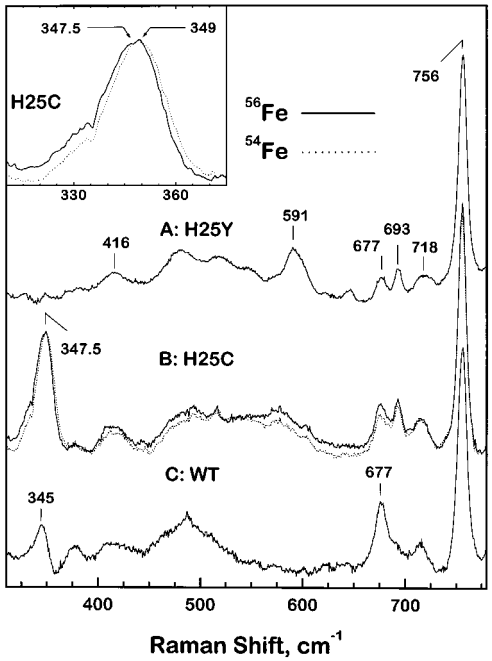

FIGURE 3: Low-frequency region of the RR spectra of ferric H25Y (A), H25C (B), and wild-type (C) hHO-1·heme complexes. Spectra were obtained at room temperature with a 514.5-nm excitation (40 mW). The inset is a blowup of the Fe isotope sensitivity of the $\nu_{Fe-S}(Cys^-)$ in the H25C mutant.

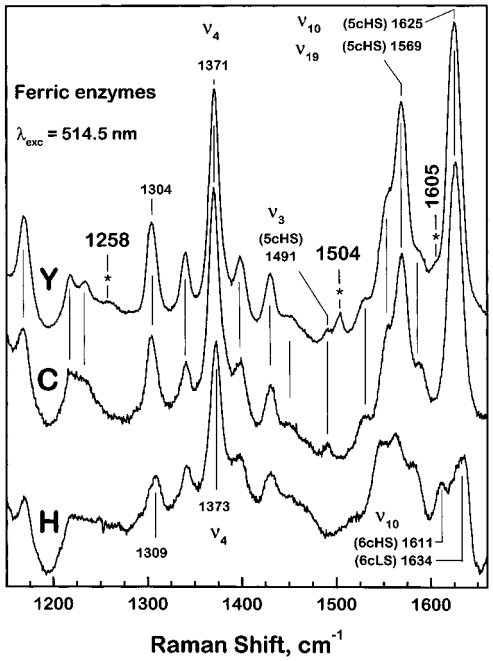

FIGURE 4: High-frequency region of the RR spectra of the ferric H25Y (Y), H25C (C), and wild-type (H) heme·hHO-1 complexes. Spectra were obtained at room temperature with 514.5-nm excitation (20 mW). Vibrational modes only observed in the spectrum of H25Y and assigned to tyrosinate vibrations are marked with an asterisk.

5-coordinate high-spin configuration (ν_2 at 1570, ν_3 at 1490, ν_4 at 1371, ν_{10} at 1626, ν_{11} at 1555, and ν_{19} at 1569 cm^{-1}). The high-frequency RR signatures of H25C and H25Y are very similar to those for the 5cHS proximal H25A hHO-1 mutant, where the heme iron is proposed to be coordinated to a single water molecule (*21*, *22*).

Nature of the Axial Ligand in the Ferric Mutant H25C and H25Y Heme·hHO-1 Complexes. RR studies of heme proteins with cysteinate or tyrosinate as proximal ligands have shown that excitation wavelengths away from the Soret absorption can result in resonance enhancement of these iron-ligand stretching vibrations. For example, the 5cHS ferric heme of cytochrome P450 shows a RR vibration at 351 cm^{-1} sensitive to iron and sulfur isotopic substitution (*37*). This Fe−S$^-$ stretching mode is resonance-enhanced with excitation wavelengths around 540 and 365 nm at which Fe−thiolate charge-transfer transitions occur (*38*). In tyrosinate ligated ferric hemes, as in Hb M Iwate and Hyde Park or in myoglobin mutants, Fe−O(Tyr$^-$) stretching modes at ∼590 cm^{-1} are resonance-enhanced with 488-nm excitation (*39*−*41*). Figure 3 shows the low-frequency region of the RR spectra of hHO-1 wild-type, H25C, and H25Y obtained with 514.5-nm excitation. In H25C, an intense band at 347.5 cm^{-1}, not observed in other forms of hHO-1 and upshifted by 1.5 cm^{-1} in the ^{54}Fe-labeled enzymes, is assigned to an Fe−S(cysteinate) stretching mode.[3] At the same excitation wavelength, no such vibration is observed in H25Y; however, a distinct new RR band is seen at 591 cm^{-1}. Although this latter mode does not show a significant shift upon ^{54}Fe substitution, it can be assigned to the Fe−O stretching mode that is strongly coupled with phenolate ring vibrations (*39*, *42*). The iron−tyrosinate binding is further confirmed by observing resonance-enhanced tyrosinate ring modes at 1504 and 1605 cm^{-1} (Figure 4). In hemoglobin and myoglobin with tyrosinate as the axial ligand, a RR band at ∼1300 cm^{-1} was assigned to $\nu_{(C-O)}$ of the phenolate (*39*−*41*). This assignment may be questioned since a porphyrin vinyl in-plane C−H bending mode occurs at the same frequency (*43*) and such a band is observed in wild-type hHO-1 as well as the two mutant proteins (Figure 4). Instead, we assign the $\nu_{Tyr(C-O)}$ to a RR band at 1258 cm^{-1}; it is only observed in the H25Y mutant and is consistent with previous work on catalases where this mode is reported at ∼1244 cm^{-1} (*44*, *45*). These results indicate that binding of the heme in the H25C and H25Y hHO-1 mutants takes place in the same substrate pocket as in the wild-type enzyme. However, whereas a water molecule is stabilized in the distal pocket of the native enzyme, resulting in a 6-coordinated heme, ligation of the iron to a cysteinate or tyrosinate side chain in the mutants produces a 5cHS configuration. The same behavior was observed in the H93C and H93Y (F8) proximal mutants of human myoglobin, which exhibit a 5cHS ferric rather than the 6cHS configuration of aquometmyoglobin in wild-type Mb (*40*).

Ferrous and Ferrous−CO Complexes of the H25C and H25Y Heme·hHO-1 Complexes. The high-frequency region of the RR spectra of the ferrous hHO-1 mutants obtained with Soret and Q-band excitation are shown in Figure 5. These spectra clearly indicate a mixture of 5cHS and 4c intermediate-spin (IS) ferrous hemes in both mutants (ν_2 at 1562 and 1580, ν_3 at 1472 and 1501, ν_4 at 1357 and 1369, ν_{10} at 1606 and 1638 cm^{-1}), as previously observed in the H25A hHO-1 mutant (*21*). In H25C, neither of the ν_4

[3] We believe that the 345 cm^{-1} band observed in wild-type hHO-1 arises from the hexacoordinate species. No such band is observed in pentacoordinate H25Y. Thus, the 347 cm^{-1} band in pentacoordinate H25C is unique to the cysteine-ligated mutant. Similarly, the ν(Fe−S) of cytochrome P450 is observed only in the 5cHS ferric, substrate-bound enzyme at ∼350 cm^{-1}.

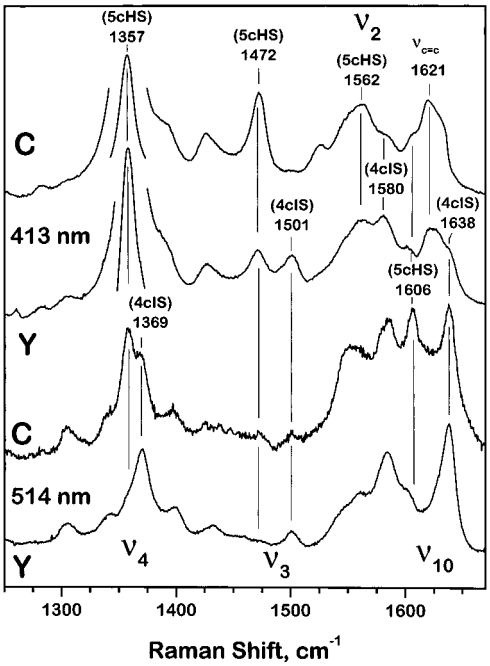

FIGURE 5: High-frequency region of the RR spectra of the ferrous H25C (C) and H25Y (Y) heme·hHO-1 complexes. Spectra were obtained at room temperature with 413 (5 mW) and 514.5-nm excitation (20 mW).

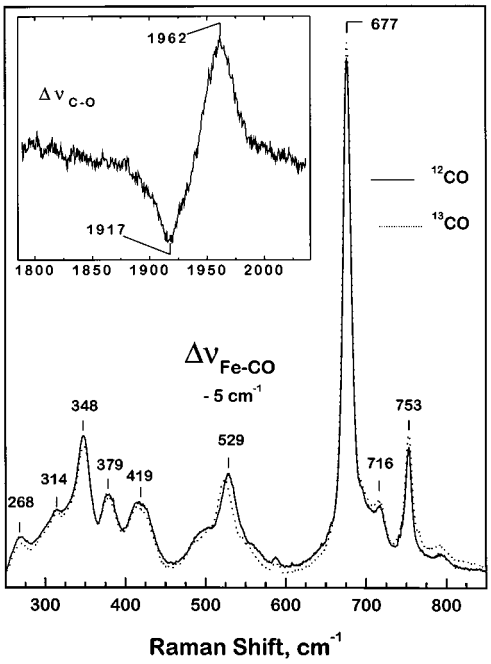

FIGURE 6: Low-frequency region of the RR spectra of the ferrous−CO H25Y heme·hHO-1 complex with ^{12}CO (—) or ^{13}CO (···). The inset shows the difference spectrum (^{12}CO − ^{13}CO) in the high-frequency region. The same experiment conducted with H25C gave identical results.

vibrations at 1369 cm^{-1} (4cIS) and 1357 cm^{-1} (5cHS) is consistent with Fe^{II}−thiolate hemes which have unique ν_4 modes at ∼1350 cm^{-1} (*45*). From these observations we can conclude that the Fe−Cys^- and Fe−Tyr^- bonds are lost upon reduction, and the ferrous heme is only loosely bound to a very weak ligand, perhaps a water molecule. Upon exposure to CO the two mutant samples present similar absorption spectra with Soret maxima at ∼412 nm and Q-bands at ∼536 and 566 nm. The Fe−CO vibrational modes of the CO complexes were identified by $^{12}C/^{13}C$ isotopic substitution (Figure 6). The ν_{Fe-CO} is observed at 529 cm^{-1} (downshifts 5 cm^{-1} with ^{13}CO) and the ν_{CO} at 1962 cm^{-1} (downshifts 45 cm^{-1} with ^{13}CO). These frequencies are identical to those observed in the H25A hHO-1 mutant (*21*) and are characteristic of a heme−CO complex with a very weak (e.g., H_2O) or no proximal ligand (*46*, *47*). Our RR data show that the cysteinate or tyrosinate ligation observed in the ferric states of the mutated enzymes is lost upon reduction, resulting in a heme configuration identical to that in the H25A hHO-1 mutant in which there is no proximal ligand to the heme iron.

Catalytic Turnover of the H25C and H25Y Heme·hHO-1 Complexes. Addition of NADPH and cytochrome P450 reductase to either the H25C or H25Y heme·hHO-1 complex under a CO atmosphere results in rapid formation of the ferrous−CO complex with a Soret maximum at 412 nm and α- and β-bands at 566 and 536 nm, respectively (Figure 7B,C). Addition of O_2 to this reaction mixture regenerates the ferric enzyme rather than resulting, as with the wild-type enzyme, in displacement of the CO by O_2 to give the ferrous−O_2 complex with a Soret maximum at 410 nm (Figure 7). In the wild-type hHO-1 complex, formation of the ferrous−oxy complex is followed by formation of the ferrous−verdoheme−CO complex with absorption at 640 nm and, subsequently, the final biliverdin product with a broad absorption centered at 680 nm (Figure 7A). In neither mutant is the verdoheme−CO complex formed, although the heme is slowly destroyed, presumably by the autoxidatively generated H_2O_2 (Figure 7). No more than a trace of biliverdin is detected in these samples by HPLC analysis. Thus, the H25C and H25Y heme·hHO-1 complexes retain the ability to accept the first electron from NADPH-cytochrome P450 reductase, but normal turnover is subsequently blocked. The behavior of these two mutants is similar to that of the H25A heme·hHO-1 complex, which produces a ferrous−CO complex with NADPH/P450 reductase that reverts to the ferric state when O_2 is added (*22*).

Uncoupled Turnover of the H25C, H25Y, and H25A Heme·hHO-1 Complexes. The ferrous−O_2 complexes of these proximal ligand mutants presumably autoxidize to generate superoxide, which disproportionates to H_2O_2 and H_2O. To test this proposal, the rate of autoxidation of the wild-type, H25C, H25Y, and H25A heme·hHO-1 complexes were determined by measuring the rate of H_2O_2 formation (Table 1). For wild-type hHO-1 and the three proximal mutants, the ratio of the NADPH and O_2 consumption rates is approximately 1:1, indicating that oxygen only undergoes a two-electron reduction. The proportion of the coupled versus uncoupled pathway does not depend on whether stoichiometric or substoichiometric amounts of cytochrome P450 reductase are present, suggesting that H_2O_2 formation involves autoxidation of the ferrous dioxy heme oxygenase complex and is not simply due to reoxidation of the P450 reductase by O_2. The H25C, H25Y, and H25A mutations significantly alter the proportion of the coupled and uncoupled pathways (Table 1). For wild-type hHO-1, ∼11−17% of the NADPH consumed was utilized in the formation of H_2O_2. However, 39−45% of the NADPH was uncoupled to form H_2O_2 with the three mutants. This finding is consistent with the electronic spectroscopic data showing that the mutant complexes are readily reduced by NADPH−

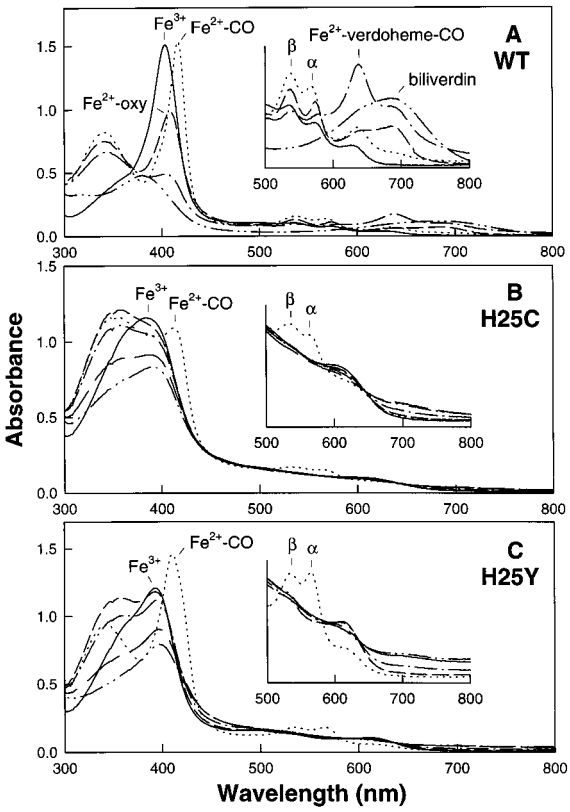

FIGURE 7: Spectroscopic changes occurring during catalytic turnover of the wild-type (A), H25C (B), and H25Y (C) heme·hHO-1 complexes with NADPH−cytochrome P450 reductase. The inset in each panel is a 5-fold expansion in the absorbance of the region between 500 and 700 nm. The turnover reaction was performed by adding NADPH to 10 μM heme·hHO-1 complex in the presence of 0.5 μM P450 reductase. For each protein, the spectra shown are of ferric heme oxygenase (—) and the heme oxygenase complex at the times indicated after addition of NADPH under a CO atmosphere (···) and under an O_2 atmosphere: immediately (- - -), 40 s (— · —), 4 min (— — —), and 8 min (— ·· —). The 4 min trace is not shown in panel (A) to minimize the congestion in the figure.

cytochrome P450 reductase without the detectable formation of verdoheme or biliverdin.

Reaction of the H25C and H25Y Heme·hHO-1 Complexes with H_2O_2. Addition of 1 equiv of H_2O_2 to the H25C heme·hHO-1 complex causes the Soret band to shift from 385 to 395 nm and to decrease in intensity (Figure 8B). The broad 500−550 nm band in the visible region is also lost. Further addition of H_2O_2 causes a gradual loss of the Soret intensity without a further shift of the Soret maximum. The same results are obtained whether H_2O_2 is added under aerobic or anaerobic conditions. Thus, in contrast to the results with wild-type hHO-1 (*18*), no detectable α-*meso*-hydroxyheme or verdoheme is formed with the H25C heme·hHO-1 complex. The initial product of the reaction of H_2O_2 with the H25C heme·hHO-1 complex is not known. It does not appear to be the ferryl species because addition of phenol, potassium ferrocyanide, or sodium dithionite causes no change in the UV−vis spectrum (data not shown). The RR spectrum before and after reaction of H_2O_2 with the H25C heme·hHO-1 complex was also examined. After the H_2O_2 reaction, the heme remains 5cHS. However, the 347.5 cm^{-1} band of the Fe−thiolate disappears (data not shown), indicating that the Fe−thiolate bond is lost. One explanation for this loss is that the H_2O_2 oxidizes the proximal thiolate ligand to cysteic acid. The H25Y heme·hHO-1 complex is insensitive to the addition of 1−3 equiv of H_2O_2, as only minor changes are observed in UV−vis (Figure 8C) and RR spectra. The reason there is no reaction of the H25Y heme·hHO-1 complex with H_2O_2 is unclear, but it suggests that H_2O_2 is unable to bind to the distal side of the iron in the mutated active site.

Reduction Potential Measurements. The H25A, H25C, and H25Y mutants fail to oxidize heme to biliverdin but retain the ability to accept the first, but apparently not second, electron from NADPH−cytochrome P450 reductase. The reduction potentials of the wild-type, H25C, and H25A heme·hHO-1 complexes have therefore been measured (Table 2). The spectra of the potentiometric titration of wild-type hHO-1 are shown in Figure 9A. The reduction of ferric to ferrous hHO-1, as reported by Sun et al. (*20*), red-shifts the Soret band from 405 to 430 nm. The midpoint reduction potential determined from Nernst plots based on the absorbance at 405 nm was -65 ± 1 mV (slope $= 63 \pm 1$ mV). The result obtained from the data at 430 nm is within experimental error of that at 405 nm. This potential is significantly lower than that of myoglobin (55.9 ± 0.1 mV, pH 7.5, 25 °C) (*48*), a protein with spectroscopic properties similar to those of heme oxygenase.

Replacement of the proximal histidine by an alanine drastically alters the electrochemical behavior of the protein. The heme in the H25A hHO-1 mutant is 5-coordinate in the ferric state and both 4- and 5-coordinate in the ferrous state, with a water molecule as the axial ligand in both oxidation states (*21*). Reduction of the H25A heme·hHO-1 complex results in a red shift of the Soret band from 400 to 426 nm (Figure 9B). Unlike the wild-type enzyme, the Soret band of the ferrous H25A heme·hHO-1 complex is more intense than that of the ferric form, and the isosbestic points are less well defined. The midpoint potential, calculated from the change in absorbance at 426 nm, is -105.9 ± 1.7 mV (Nernst slope 59.2 ± 2.0). The potential calculated from the changes at 400 nm is ∼16 mV higher. The reason for this difference is unknown, but it could signal the presence of more than two electroactive chromophores.

When a large (>200-fold) excess of imidazole is added to the ferric H25A heme·hHO-1 complex, the Soret band shifts from 400 to 413 nm, consistent with formation of the bis(imidazole) heme complex. The spectrum of this complex resembles that of ferricytochrome b_5 (*49*). The spectroelectrochemical data (Figure 9C) for this species reveal distinct isosbestic points with a midpoint reduction potential derived from the Soret band of -176.9 ± 1.6 mV (Nernst slope 64.0 ± 2.7). If the change in absorbance of the Soret band of the reduced form is used, the calculated potential is approximately 6 mV lower. Interestingly, reduction of the bis(imidazole) form shifts the Soret band to 426 nm, a position that is similar to that of ferrocytochrome b_5 (*49*). This behavior contrasts with that of the imidazole complex of metmyoglobin, which converts to a 5-coordinate (deoxy) species (Soret maximum 435 nm) upon reduction.

If a 40-fold molar excess of imidazole is added to ferric H25A heme·hHO-1 complex, the Soret shifts from 400 to 405 nm. The similarity of the latter to the spectrum of wild-type heme oxygenase indicates that its heme is 6-coordinate and possesses imidazole and water as axial ligands. The family of spectra obtained from the spectroelectrochemical

Table 1: Uncoupled Oxidation of the Heme Complexes of Wild-Type, H25C, H25Y, and H25A hHO-1

proteins[a]	P450- reductase[b] (%)	−d[NADPH]/d*t*[c] (μM min^{-1})	−d[O_2]/d*t* w/o catalase[c] (μM min^{-1})	−d[O_2]/d*t* w/catalase[c,d] (μM min^{-1})	+d[H_2O_2]/d*t* (μM min^{-1})	uncoupled (%)
hHO-1	1.75	9.77	10.42	9.79	1.25	12.8
	3.5	19.18	17.92	16.88	2.08	10.8
	50	19.74	17.71	16.04	3.33	16.8
	100	36.02	31.04	28.13	5.83	16.2
H25C	3.5	8.98	6.83	4.91	3.84	42.7
	50	12.38	11.77	9.01	5.52	44.6
	100	24.00	22.52	17.08	10.88	45.3
H25Y	1.75	10.54	6.83	4.48	4.69	44.5
	3.5	18.40	11.95	8.10	7.68	41.7
	50	17.97	13.44	9.81	7.25	40.4
	100	31.35	23.04	16.43	13.23	42.2
H25A	1.75	7.30	6.39	4.85	3.08	42
	3.5	14.5	13.17	10.36	5.62	39
	50	15.43	14.32	10.93	6.78	44
	100	29.17	26.74	20.45	12.58	43.1

[a] Reaction conditions are described under Experimental Procedures. [b] hHO-1 (5 μM) was used for the reaction with substoichiometric amounts of P450 reductase (1.75% and 3.5%), and 1 μM hHO-1 was used for the reaction with stoichiometric amounts of P450 reductase (50% and 100%), respectively. [c] Both NADPH and O_2 consumption rates were measured at 25 °C, pH 7.4. [d] A catalytic amount of catalase (5% relative to hHO-1) was included in the reaction.

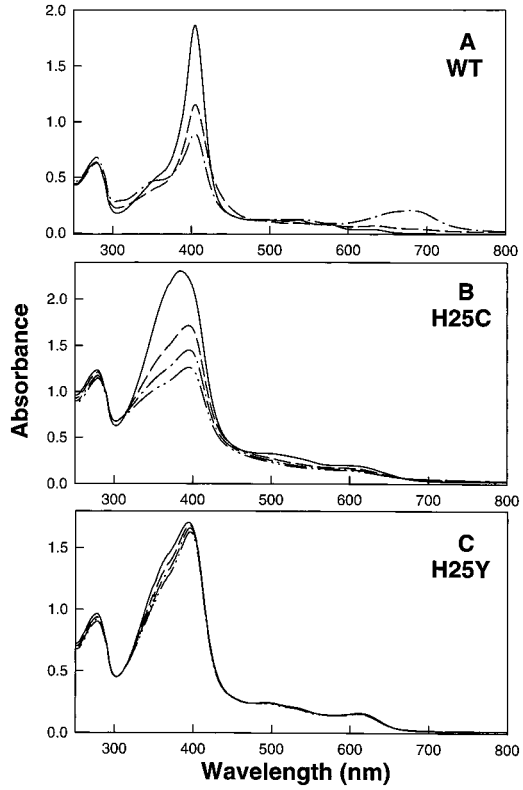

FIGURE 8: UV−vis spectra of the reaction with H_2O_2 of the wild-type (A), H25C (B) and H25Y (C) hHO-1:heme complexes. (A) Formation of the α-meso-hydroxyheme·hHO-1 complex (- - -) and verdoheme·hHO-1 complex (- · -) by, respectively, anaerobic and aerobic addition of 1 equiv of H_2O_2 to the wild-type heme·hHO-1 (—) complex. (B, C) Aerobic addition of 1 (- - -), 2 eq (— · —), and 3 equiv (— ·· —), respectively, of H_2O_2 to the H25C and H25Y hHO-1·ferric heme (—) complexes, respectively. The same results are obtained if the reactions are carried out anaerobically.

titration, however, differs from that of wild-type heme oxygenase (Figure 9D). This fact, combined with the poor isosbestic points, suggests that this derivative may undergo an oxidation state-dependent change in axial ligation. It is likely that the K_D values of the imidazole−ferric and −ferrous heme complexes differ enough that it may be difficult to reach the same active-site imidazole stoichiometry in both oxidation states by adding controlled amounts of imidazole. A difference in the imidazole bound fraction in the two oxidation states would complicate the potentiometric titration and prevent the determination of a precise midpoint potential with a lower Nernst slope error (Table 2).

Table 2: Parameters Derived from Spectroelectrochemical Measurements of Wild-Type and Mutant Human Heme Oxygenase Forms (25 °C)

	oxidized		reduced	
protein	potential (mV vs SHE)	slope (mV)	potential (mV vs SHE)	slope (mV)
hHO-1	−65 ± 1	63 ± 1	−67 ± 1	64 ± 1
H25A	−90 ± 2	45 ± 1	−106 ± 2	59 ± 2
H25A-$(Im)_1$	−54 ± 2	71 ± 3	−118 ± 1	74 ± 1
H25A-$(Im)_2$	−177 ± 2	64 ± 3	−183 ± 1	55 ± 2
H25C	−150	85		

For the heme·H25C complex, the spectra obtained from the potentiometric titration do not show a clean isosbestic point. As discussed earlier, RR data show that the Fe−S ligation of the complex is lost upon reduction to the ferrous state. Thus, it will be difficult to determine its precise reduction potential. The results show that the approximate potential for the H25C mutant is −150 mV versus SHE at 23 °C, pH 7.4, but the Nernst slope value of 85 indicates that there is significant error in the measurement.

DISCUSSION

The H25C and H25Y hHO-1 mutants are expressed as folded proteins that can be reconstituted with heme to give spectroscopically intact heme−protein complexes. RR studies provide strong evidence that the proximal ligands in the two ferric heme·protein complexes are, respectively, a cysteine thiolate and a tyrosine phenoxide. However, the RR spectra also show that the Fe−Cys and Fe−Tyr ligation is lost in the H25C and H25Y heme complexes, respectively, when the iron is reduced to the ferrous state (Figures 5 and 6). Dissociation of the proximal ligand in the ferrous state is confirmed by the finding that the absorption maximum of

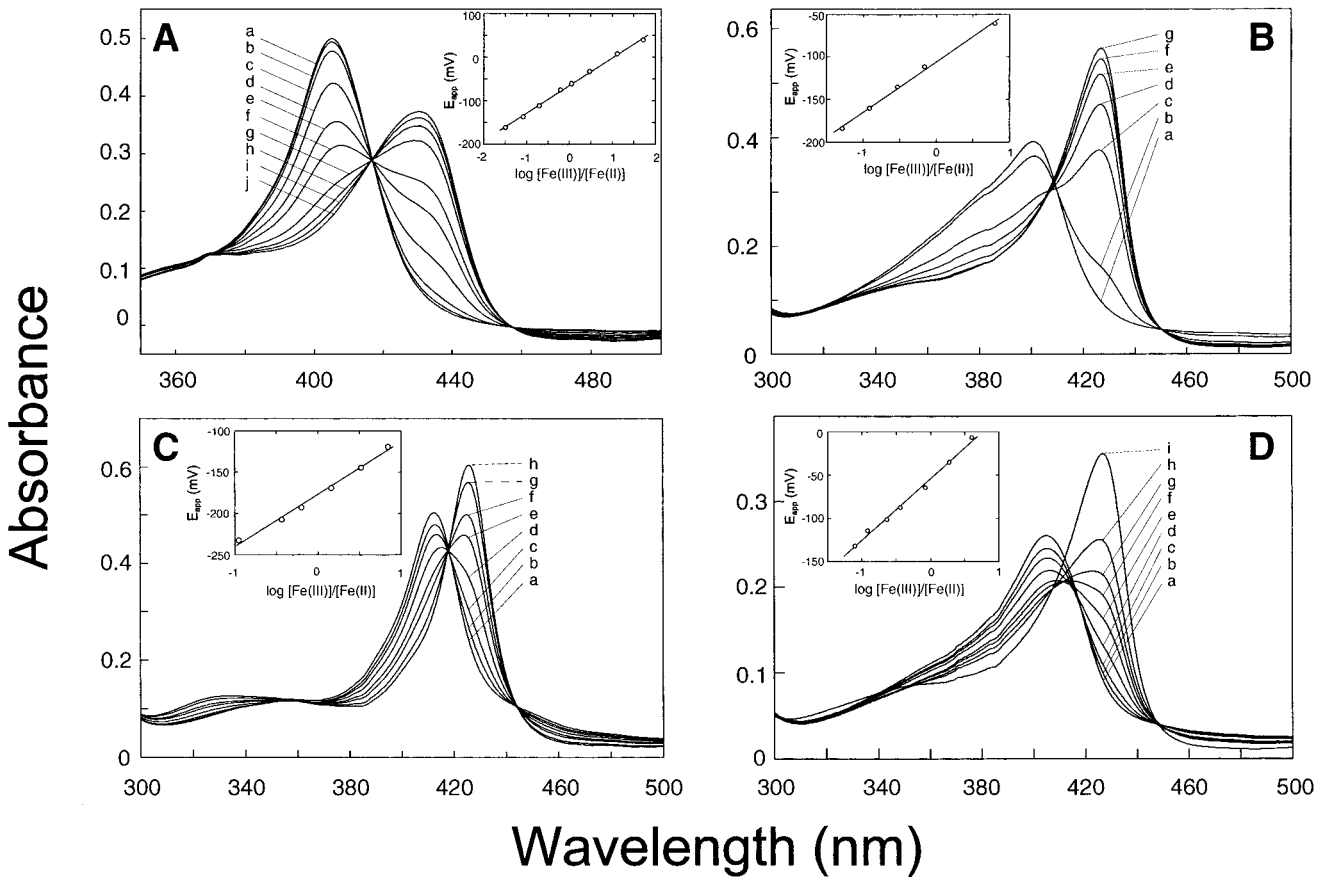

FIGURE 9: UV−vis spectra of the reduction titration of the heme·hHO-1, H25A heme·hHO-1, H25A heme·hHO-1 mono- and bis(imidazole) complexes, respectively. (A) Spectroelectrochemical titration of the wild-type heme·hHO-1 complex (∼90 μM protein in 20 mM potassium phosphate buffer, pH 7.4, 25 °C). The solution potential corresponding to each spectrum is as follows (in millivolts vs SHE): (a) 437, (b) 39, (c) 7, (d) 33, (e) −61, (f) −75, (g) −111, (h) −136, (i) −161, and (j) −259. The inset is a Nernst plot derived from the change in absorbance at 405 nm. (B) Spectroelectrochemical titration of the H25A heme·hHO-1 complex (∼100 μM protein in 20 mM potassium phosphate buffer, pH 7.4, 25 °C). The solution potential corresponding to each spectrum is as follows (in millivolts vs SHE): (a) 341, (b) −61, (c) −112, (d) −135, (e) −161, (f) −184, and (g) −321. The inset is a Nernst plot derived from the change in absorbance at 426 nm. (C) Spectroelectrochemical titration of the bis(imidazole) complex of the H25A heme·hHO-1 complex (∼93 μM protein and 40 mM imidazole in 20 mM potassium phosphate buffer, pH 7.4, 25 °C). The solution potential corresponding to each spectrum is as follows (in millivolts vs SHE): (a) 413, (b) −119, (c) −144, (d) −169, (e) −193, (f) −207, (g) −233, and (h) −285. The inset is a Nernst plot derived from the change in absorbance at 412 nm. (D) Spectroelectrochemical titration of the monoimidazole complex of the H25A heme·hHO-1 complex (∼97 μM protein and 4 mM imidazole in 20 mM potassium phosphate buffer, pH 7.4, 25 °C). The solution potential corresponding to each spectrum is as follows (in millivolts vs SHE): (a) 427, (b) −7, (c) −35, (d) −64, (e) −87, (f) −101, (g) −114, (h) −132, and (i) −246 mV (fully reduced) (SHE). The Nernst plot was derived from the dependence of the absorbance at 405 nm on the solution potential.

the H25C ferrous−CO complex is not at approximately 450 nm. Moreover, the correlation between $\nu_{(CO)}$ and $\nu_{(Fe-CO)}$ in this complex indicates the absence of a strong fifth ligand. Dissociation of the proximal iron ligand thus yields an enzyme with an iron ligation state similar to that of the previously characterized H25A mutant (*21*, *22*).

The exact reason for loss of the Fe−thiolate and Fe−tyrosinate ligand upon reduction of the heme iron is not known. Reduction may favor protonation of the thiolate or tyrosinate ligand, thus weakening the Fe−S or Fe−O bond and leading to dissociation of the ligand. This could be due not only to the electrostatic change in the iron−thiolate or iron−phenolate interaction but also to the fact that the geometry required for coordination of the thiolate or phenolate ion is not optimum and may be more sensitive to redox-mediated protein conformational changes.[4] Poulos has pointed out that the cysteine thiolate in P450 enzymes may be stabilized by its location at the N-terminal end of the proximal helix, which places it near the N-terminal end of the helical dipole (*50*). The proximal histidine in the peroxidases and globins is at the C-terminal end of the dipole. The location of the proximal ligand in HO-1 is not yet known, but the cysteine thiolate may also be relatively destabilized by the helix dipole if it is located at the C- rather than N-terminus of a helix.

Loss of the proximal Fe−thiolate ligand after reduction has also been demonstrated with the proximal H93C myoglobin mutant (*51*, *52*). A computer graphics analysis of the replacement of His-93 by a cysteine residue in the crystal structure of myoglobin shows that, in the absence of any compensatory changes in the protein, the Fe−S distance would be 3.9 Å rather than the more normal 2.3−2.5 Å expected for such a bond (*52*). A similar discrepancy in the optimal Fe−S bond distance is likely to occur in the hHO-1

[4] Efforts to prevent protonation of the thiolate ligand by increasing the pH from 7 to 13 were unsuccessful because at all pH values the ferrous−CO absorbance maximum was at 412 rather than 450 nm (not shown). Even when the H25C apoprotein was reconstituted at pH 9, 11, or 13 with ferrous heme under a CO atmosphere, no 450-nm absorbing species was observed (not shown). The pH insensitivity of the chromophore is therefore not due to limited solvent accessibility to the proximal pocket in the heme-containing protein.

mutants unless the protein can relax sufficiently to allow the cysteine thiolate to more closely approach the iron atom.

A key consequence of proximal ligand dissociation upon reduction of the H25C and H25Y heme•hHO-1 complexes is that, in contrast to the wild-type complex, the two mutants fail to form stable ferrous−dioxy complexes. Instead, the ferrous mutant proteins autoxidize to the ferric state, as observed previously with the H25A heme•hHO-1 complex. The stability of the ferrous−O_2 complex reflects interactions of the iron-bound dioxygen with distal active-site residues, the polarity of the distal cavity, and the electronic properties of the proximal heme ligand. The absence of a proximal iron ligand can electronically perturb the ferrous−dioxy complex, thus preventing its formation, destabilizing the complex sufficiently that reduction becomes noncompetitive with respect to dissociation of protonated superoxide, or preventing the second electron transfer from NADPH−cytochrome P450 reductase to the ferrous−dioxy complex.

The amount of H_2O_2 formed by the three proximal mutants does not account for all the NADPH that is consumed. Approximately ∼50% of the NADPH consumed remains unaccounted for because no verdoheme or biliverdin is detectably formed. The possibility that the H_2O_2 assay is inaccurate is ruled out by control experiments in which known amounts of H_2O_2 were added to the standard assay mixture (excluding NADPH). The amount of oxygen measured in these control studies agreed with the amount expected from the H_2O_2 added, which indicates that the H_2O_2 assay is correctly reporting the H_2O_2 concentration. Control experiments also show that H_2O_2 reacts much faster with catalase than with heme oxygenase. The possibility that the enzyme reduces O_2 all the way to water, as partially occurs with cytochrome P450 (*53*−*55*), is ruled out by the 1:1 stoichiometry of NADPH and O_2 consumed and the fact that a ferryl intermediate is not involved in the heme oxygenase α-*meso*-hydroxylation reaction. The additional NADPH consumption may be related to the formation of heme degradation products other than biliverdin.

The reduction potential of the wild-type heme•hHO-1 complex (−65 mV) is more negative than that of myoglobin (+56 mV) (*56*) but is more positive than that of cytochrome *c* peroxidase (−194 mV) (*57*), horseradish peroxidase (−250 mV) (*58*), or substrate-free cytochrome $P450_{cam}$ (−300 mV) (*59*). These reduction potential values appear to correlate with the electronic properties of the axial iron ligand, with the stronger electron-donating ligand giving the most negative reduction potential. Replacement of the proximal histidine ligand by an alanine (−106 mV) or cysteine (−150 mV) causes the reduction potential to shift to more negative values, which indicates that reduction of the iron becomes thermodynamically less favorable compared to reduction of the iron in the wild-type enzyme. It must be borne in mind, however, that the coordination state of the alanine and cysteine mutants differs and therefore that a simple comparison of the factors that control the reduction potentials in the two proteins is not straightforward. Despite the differences, the potential values of the proteins are still significantly more positive than that of cytochrome P450 reductase ($E^{0'} = -270$ mV for $1e^-$ to $2e^-$ and −290 mV for $2e^-$ to $3e^-$) (*60*), which indicates that reduction of heme oxygenase by P450 reductase remains thermodynamically favorable. This is consistent with the observation that both mutants are reduced by NADPH−cytochrome P450 reductase, although the reduction rates may differ. This observation suggests that destabilization of the ferrous dioxygen complex is the probable reason for loss of heme oxygenase activity when there is no heme proximal ligand, as in the ferrous H25A, H25C, and H25Y heme•hHO-1 complexes.

Scheme 2: Proposed Pathway for Autoxidation of the Heme•hH25C Complex in the Presence of NADPH−Cytochrome P450 Reductase[a]

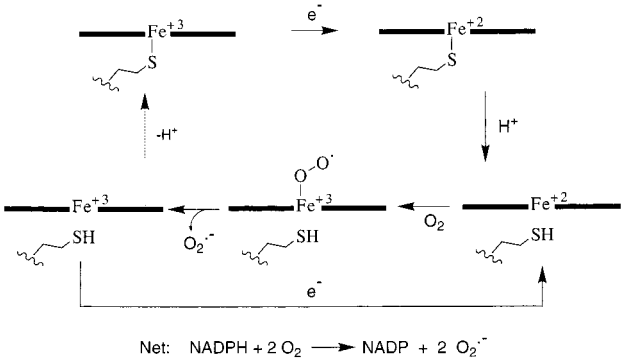

[a] A similar scheme can be written for the H25Y mutant with a tyrosine hydroxyl replacing the cysteine ligand. After dissociation of the thiolate ligand, the autooxidative cycle may proceed, as in the H25A mutant, without re-formation of the cysteine thiolate−iron complex.

In summary, mutagenesis of the hHO-1 proximal histidine to a cysteine or a tyrosine yields ferric axial ligation states that resemble those in cytochrome P450 and catalase, respectively. Coordination of the cysteine and tyrosine to the ferric heme is confirmed by RR spectroscopy, which also establishes that the iron is in a high-spin, 5-coordinate state. The reduction potential of the ferric/ferrous couple for the heme•H25C complex is more negative than that for wild-type hHO-1 due to coordination of a more electronegative ligand to the iron. Nevertheless, the first electron transfer to the heme•H25C complex by P450 reductase remains thermodynamically favorable and the heme•H25C and H25Y mutants are reduced by NADPH-cytochrome P450 reductase. The properties of the ferrous heme•H25C and H25Y CO complexes indicate that the cysteine and tyrosine ligands are lost upon reduction of the iron. Loss of the proximal ligand upon reduction interferes with the binding of O_2 or the stability of the resulting ferrous−dioxy complex. Thus, both the H25C and H25Y heme•hHO-1 complexes fail to form detectable ferrous−dioxy intermediates and both, like the H25A mutant, undergo uncoupled turnover to form H_2O_2 (Scheme 2). Rapid autoxidation of the heme•hHO-1 complex due to loss of the proximal ligand in the H25C and H25Y mutants converts these proteins from heme oxygenases to oxidases that catalyze the NADPH−dependent reduction of O_2 to H_2O_2.

REFERENCES

1. Tenhunen, R., Marver, H. S., and Schmid, R. (1969) *J. Biol. Chem. 244*, 6388−6394.
2. Poss, K. D., and Tonegawa, S. (1997) *Proc. Natl. Acad. Sci. U.S.A. 94*, 10919−10924.
3. Schmid, R., and McDonagh, A. F. (1979) in *The Porphyrins* (Dolphin, D., Ed.) Vol. VI, pp 257−292, Academic, New York.
4. Stocker, R., Yamamoto, Y., McDonagh, A. F., Glazer, A. N., and Ames, B. N. (1987) *Science 235*, 1043−1046.

5. Maines, M. D. (1992) *Heme Oxygenase: Clinical Applications and Functions*, pp 109−144, CRC Press, Boca Raton, FL.
6. Maines, M. D., and Trakshel, G. M. (1992) *Biochim. Biophys. Acta 1131*, 166−174.
7. Kappas, A., Drummond, G. S., Manola, T., Petmezaki, S., and Values, T. (1988) *Pediatrics 81*, 485−497.
8. Drummond, G. S., and Kappas, A. (1981) *Proc. Natl. Acad. Sci. U.S.A. 78*, 6466−6470.
9. Verma, A., Hirsch, D. L., Glatt, C. E., Ronnett, G. V., and Snyder, S. H. (1993) *Science 259*, 381−384.
10. Stevens, C. F., and Wang, Y. (1993) *Nature 364*, 147−149.
11. Burnett, A. L., Johns, D. G., Kriegsfield, L. J., Klein, S. L., Calvin, D. C., Demas, G. E., Schramm, L. P., Tonegawa, S., Nelson, R. J., Snuder, S. H., and Poss, K. D. (1998) *Nat. Med. 4*, 84−87.
12. Zakhary, R., Poss, K. D., Jaffrey, S. R., Ferris, C. D., Tonegawa, S., and Snyder, S. H. (1997) *Proc. Natl. Acad. Sci. U.S.A. 94*, 14848−14853.
13. Maines, M. D., Trakshel, G. M., and Kutty, R. K. (1986) *J. Biol. Chem. 261*, 411−419.
14. Maines, M. D. (1988) *FASEB J. 2*, 2557−2568.
15. McCoubrey, W. K., Huang, T. J., and Maines, M. D. (1997) *Eur. J. Biochem. 247*, 725−732.
16. Yoshida, T., Biro, P., Cohen, T., Müller, R. M., and Shibahara, S. (1988) *Eur. J. Biochem. 171*, 457−461.
17. McCoubrey, W. K., and Maines, M. D. (1993) *Arch. Biochem. Biophys. 302*, 402−408.
18. Wilks, A., and Ortiz de Montellano, P. R. (1993) *J. Biol. Chem. 268*, 22357−22362.
19. Wilks, A., Black, S. M., Miller, W. L., and Ortiz de Montellano, P. R. (1995) *Biochemistry 34*, 4421−4427.
20. Sun, J., Wilks, A., Ortiz de Montellano, P. R., and Loehr, T. M. (1993) *Biochemistry 32*, 14151−14157.
21. Sun, J., Loehr, T. M., Wilks, A., and Ortiz de Montellano, P. R. (1994) *Biochemistry 33*, 13734−13740.
22. Wilks, A., Sun, J., Loehr, T. M., and Ortiz de Montellano, P. R. (1995) *J. Am. Chem. Soc. 117*, 2925−2926.
23. Takahashi, S., Wang, J., Rousseau, D. L., Ishikawa, K., Yoshida, T., Host, J. R., and Ikeda-Saito, M. (1994) *J. Biol. Chem. 269*, 1010−1014.
24. Takahashi, S., Wang, J., Rousseau, D. L., Ishikawa, K., Yoshida, T., Takeuchi, N., and Ikeda-Saito, M. (1994) *Biochemistry 33*, 5531−5538.
25. Ito-Maki, M., Ishikawa, K., Matera, K. M., Sato, M., Ikeda-Saito, M., and Yoshida, T. (1995) *Arch. Biochem. Biophys. 317*, 253−258.
26. Gerber, N. C., and Sligar, S. G. (1992) *J. Am. Chem. Soc. 114*, 8742−8743.
27. Wilks, A., Torpey, J. and Ortiz de Montellano, P. R. (1994) *J. Biol. Chem. 269*, 29553−29556.
28. Sambrook, J., Fritsch, E. F., and Maniatis, T. (1989) *Molecular Cloning: A Laboratory Manual*, Cold Spring Harbor Laboratory Press, Cold Spring Harbor, NY.
29. Liu, Y., Moënne-Loccoz, P., Loehr, T. M., and Ortiz de Montellano, P. R. (1997) *J. Biol. Chem. 272*, 6909−6917.
30. Ramettes, R. W., and Stanford, R. W., Jr. (1965) *J. Am. Chem. Soc. 82*, 5001−5005.
31. Wagner, G. C., Perez, M., Toscano, W. A., Jr., and Gunsalus, I. C. (1981) *J. Biol. Chem. 256*, 6262−6265.
32. Loehr, T. M., and Sanders-Loehr, J. (1993) *Methods Enzymol. 226*, 431−470.
33. Stankovich, M. T. (1980) *Anal. Biochem. 109*, 295−308.
34. Dutton, P. L. (1978) *Methods Enzymol. 54*, 411−435.
35. Pladziewicz, J. R., Meyer, T. J., Broomhead, J. A., and Taube, H. (1973) *Inorg. Chem. 12*, 639−643.
36. Spiro, T. G., and Li, X. Y. (1988) *Biological Applications of Raman Spectroscopy. Vol. 3. Resonance Raman Spectra of Hemes and Metalloproteins* (Spiro, T. G., Ed.) Vol. 3, pp 1−37, John Wiley & Sons, New York.
37. Champion, P. M., Stallard, B. R., Wagner, G. C., and Gunsalus, I. C. (1982) *J. Am. Chem. Soc. 104*, 5469−5472.
38. Yu, N. T. (1986) *Methods Enzymol. 130*, 350−409.
39. Nagai, M., Yoneyama, Y., and Kitagawa, T. (1989) *Biochemistry 28*, 2418−2422.
40. Adachi, S., Nagano, S., Ishimori, K., Watanabe, Y., Morishima, I., Egawa, T., Kitagawa, T., and Makino, R. (1993) *Biochemistry 32*, 241−252.
41. Egeberg, K. D., Springer, B. A., Martinis, S. A., Sligar, S. G., Morikis, D., and Champion, P. M. (1990) *Biochemistry 29*, 9783−9791.
42. Pyrz, J. W., Roe, A. L., Stern, L. J., and Que, L., Jr. (1985) *J. Am. Chem. Soc. 107*, 614−620.
43. Hu, S., Smith, K. M., and Spiro, T. G. (1996) *J. Am. Chem. Soc. 118*, 12638−12646.
44. Sharma, K. D., Andersson, L. A., Loehr, T. M., Terner, J., and Goff, H. M. (1989) *J. Biol. Chem. 264*, 12772−12779.
45. Remba, R. D., Champion, P. M., Fitchen, D. B., Chiang, R., and Hager, L. P. (1979) *Biochemistry 18*, 2280−2290.
46. Ray, G. B., Li, X.-Y., Ibers, J. A., Sessler, J. L., and Spiro, T. G. (1994) *J. Am. Chem. Soc. 116*, 162−176.
47. Sun, J., Chang, C. K., and Loehr, T. M. (1997) *J. Phys. Chem. B. 101*, 1476−1483.
48. Lim, A. R. (1990) Ph.D. Dissertation, University of British Columbia, Vancouver, Canada.
49. Ozols, J., and Strittmatter, P. (1964) *J. Biol. Chem. 239*, 1018−1023.
50. Poulos, T. L., Cupp-Vickery, J., and Li, H. (1995) in *Cytochrome P450: Structure, Mechanism, and Biochemistry*, 2nd ed. (Ortiz de Montellano, P. R., Ed.) pp 125−150, Plenum Press, New York.
51. Adachi, S., Nagano, S., Ishimori, K., Watanabe, Y., and Morishima, I. (1993) *Biochemistry 32*, 241−252.
52. Hildebrand, D. P., Ferrer, J. C., Tang, H.-L., Smith, M., and Mauk, A. G. (1995) *Biochemistry 34*, 11598−11605.
53. Gorsky, L. D., Koop, D. R., and Coon, M. J. (1984) *J. Biol. Chem. 259*, 6812−6817.
54. Atkins, W. M., and Sligar, S. G. (1987) *J. Am. Chem. Soc. 109*, 3754−3760.
55. Loida, P. J., and Sligar, S. G. (1993) *Biochemistry 32*, 11530−11538.
56. Varadarajan, R., Zewer, T. E., Gray, H. B., and Boxer, S. G. (1989) *Science 243*, 69−72.
57. Conroy, C. W., Tyma, P., Daum, P. H., and Erman, J. E. (1978) *Biochim. Biophys. Acta 537*, 62−69.
58. Harbury, H. (1957) *J. Biol. Chem. 225*, 1009−1024.
59. Sligar, S. G., and Gunsalus, I. C. (1976) *Proc. Natl. Acad. Sci. U.S.A. 73*, 1078−1082.
60. Vermilion, J. L., and Coon, M. J. (1978) *J. Biol. Chem. 153*, 2694−2704.

BI982707S